Effects of Triaxial Sample Scaling on the Mechanical Behavior of Alluvial Gravels

Gilbert Girumugisha, Ph.D., M.ASCE[1]; Carlos Ovalle, Ph.D.[2]; Holger Reith[3]; and Hans Henning Stutz, Ph.D.[4]

Abstract: In practical engineering, mechanical characterization of coarse gravels is usually performed on small-scale specimens, where the maximum particle size is limited to fit the material in standard testing devices. This implies altering the original particle size distribution, which is known to influence the stress–strain behavior. However, most research on grading effects has been done after comprehensive testing on sands, and the impact of small-scaling on gravelly soils is still poorly understood. This paper presents an experimental study on the shearing response of coarse soil at different specimen scales. The main objective is to assess the impact of small-scaling methods on the stress–strain behavior of coarse alluvial soils. Scalping grading and truncation techniques were used to prepare scaled specimens. Several tests were performed using triaxial cells with specimens of 100, 150, and 800 mm diameter. The analyses indicate that volumetric dilatancy strongly decreases with specimen size, while the secant strain modulus and peak shear strength slightly increase in larger specimens. Differences are mainly related to particle size distributions and packing properties. The article discusses practical insights into the effects of small-scaling variations and their implications for characterizing gravelly materials. **DOI: 10.1061/JGGEFK.GTENG-13923.**

Introduction

Large-scale testing of coarse soils remains challenging for geotechnical engineers, mainly due to the scarcity of large devices worldwide. Thus, mechanical characterization for civil engineering applications, including foundations, embankments, dams, railway ballasts, and slope stability assessments of gravelly soils, is often based on small-scale specimens. Scaling methods involve altering the particle size distribution (PSD) by removing the coarse fraction that cannot be fitted in a representative elementary volume (REV) of material, even when using the largest triaxial (Leussink 1960; Marsal 1967; Marachi et al. 1972; Hettler and Vardoulakis 1984; Verdugo and de la Hoz 2007; Hu et al. 2011; Ovalle et al. 2014; Ning et al. 2024) or direct shear (Barton and Kjærnsli 1981; Matsuoka et al. 2001; Linero et al. 2020; Girumugisha et al. 2024) devices available. However, uncertainties persist regarding the representativeness of scaling methods in capturing the behavior of oversized materials.

[1]Dept. of Civil, Geological and Mining Engineering, Polytechnique Montreal, Montreal, QC, Canada H3T 0A3; Ph.D. Student, Research Institute on Mines and the Environment UQAT-Polytechnique, Polytechnique Montreal, Montreal, QC, Canada H3T 0A3.

[2]Associate Professor, Dept. of Civil, Geological and Mining Engineering, Polytechnique Montreal, Montreal, QC, Canada H3T 0A3; Associate Professor, Research Institute on Mines and the Environment UQAT-Polytechnique, Polytechnique Montreal, Montreal, QC, Canada H3T 0A3 (corresponding author). ORCID: https://orcid.org/0000-0002-9648-5262. Email: carlos.ovalle@polytml.ca

[3]Lecturer, Institute of Soil Mechanics and Rock Mechanics, Karlsruhe Institute of Technology, Karlsruhe D-76344, Germany.

[4]Associate Professor, Institute of Soil Mechanics and Rock Mechanics, Karlsruhe Institute of Technology, Karlsruhe D-76344, Germany. ORCID: https://orcid.org/0000-0003-3360-1243

Note. This manuscript was submitted on January 28, 2025; approved on August 18, 2025; published online on October 27, 2025. Discussion period open until March 27, 2026; separate discussions must be submitted for individual papers. This paper is part of the ***Journal of Geotechnical and Geoenvironmental Engineering***, © ASCE, ISSN 1090-0241.

The most common scaling techniques used in practice are scalping grading (Zeller and Wullimann 1957; Al-Hussaini 1970; Deiminiat et al. 2022; Girumugisha et al. 2024), parallel grading (Lowe 1964; Marachi et al. 1972; Varadarajan et al. 2003; Verdugo and de la Hoz 2007; Osses et al. 2024), and the truncation method (also known as the scalp-and-replace method) (Linero et al. 2007; Hassan et al. 2022). First, the maximum particle size (d_{max}) that can be used in a laboratory specimen should be defined based on testing standards or specific requirements for the REV (Girumugisha et al. 2024; Quiroz-Rojo et al. 2024). Then, the size fractions having a characteristic size $d > d_{max}$ are removed to form a finer PSD. In scalping, all the material presenting $d \leq d_{max}$ is sieved to generate a new PSD. Thus, the coefficient of uniformity ($C_u = d_{60}/d_{10}$) of the small-scale specimen decreases. Parallel grading, on the contrary, keeps the same C_u defining a scaling factor as $F = d_{max-field}/d_{max}$, where $d_{max-field}$ is the coarsest particle in the original soil. Then, all the size fractions are simply reduced in size by F, generating a PSD parallel to the field material. However, the scaled PSD is not always parallel in the finer fractions, since it might require grain sizes that are not available in the original soil (i.e., finer than the finest fraction in the field soil). Since scalping and parallel grading methodologies require proper sieving to create the scaled PSDs, practitioners often use the truncation method. This method considers replacing particles exceeding d_{max} by the corresponding mass of grains having $d = d_{max}$. Therefore, the shape of the field PSD within the fractions finer than d_{max} is maintained, thus avoiding sieving of the scaled specimen.

It is well known that PSD impacts the stress–strain behavior of granular soils. Under particular states (e.g., stress and relative density), well-graded soils exhibit lower void ratios than uniform ones, owing to more efficient packing provided by fine grains fitting the voids between coarser grains. Therefore, as C_u increases, the critical state line shifts toward lower void ratios in the mean effective stress space (Biarez and Hicher 1994, 1997; Daouadji et al. 2001; Muir Wood and Maeda 2008), and sheared uniformly graded soils typically exhibit higher volumetric strains and lower peak shear strengths compared with well-graded materials

(Yang and Luo 2018; Ahmed et al. 2023). This behavior has been implemented in constitutive models for crushable soils upon grading evolution (Daouadji et al. 2001; Kikumoto et al. 2010; Ovalle and Hicher 2020). On the other hand, it has been widely reported that the critical friction angle does not depend on the PSD (Li et al. 2013; Yang and Luo 2018; Cantor et al. 2018; Polanía et al. 2023). However, this assumption only holds if the characteristic particle shape, surface roughness, and grain mineralogy remain consistent across grain size fractions (Linero et al. 2019; Ovalle and Dano 2020; Carrasco et al. 2023, 2025). While these observations are widely recognized, most studies on grading effects have focused on sands and fine soils, whereas the impacts in coarse gravels are still poorly understood and often contradicting. Some researchers have claimed that the shear strength decreases in larger and coarser specimens (Zeller and Wullimann 1957; Marachi et al. 1972; Linero et al. 2007; Ovalle et al. 2014), attributing this to enhanced particle crushing. In contrast, several other studies have concluded that strength increases when the material becomes coarser (Al-Hussaini 1983; Varadarajan et al. 2003; Deiminiat et al. 2022; Hao and Pabst 2023). This apparent discrepancy might stem from inadequate material characterization ensuring fair comparisons at different scales, namely, in terms of particle shapes at different grain sizes (Linero et al. 2017), the minimum specimen REV required (Cantor and Ovalle 2025) and compaction properties. Consequently, the constraints induced by small-scaling techniques are often overlooked by practitioners, and their impacts on geotechnical designs are typically disregarded or compensated by conservative safety factors.

The main objective of this paper is to assess the impact of small-scaling methods on the stress–strain behavior of coarse gravelly soil. In this context, monotonic triaxial tests were conducted on dense alluvial gravel materials under consolidated drained conditions to explore the effects of specimen size and grading on deformation and strength characteristics. Scalping grading and truncation techniques were employed at different targeted triaxial specimen sizes, with diameters of 100, 150, and 800 mm. Packing properties and characteristic particle shapes of all tested grain sizes were characterized to establish a comparable basis. The analyses focus on dilatancy, secant stiffness, and peak and critical state friction angles. The discussion addresses practical insights into the effects of small-scaling and its implications for the characterization of gravelly materials.

Experimental Methods

Alluvial Soil Characterization

Approximately 15 tons of terrace alluvial gravel material were collected from a gravel pit near Basel in Switzerland (coordinates: 47°31'33.7″N 7°39'58.5″E). The soil has a maximum particle size $d_{\text{max–field}} = 125$ mm and less than 2% fines (finer than 80 μm). Fig. 1(a) illustrates the PSD of the sampled material, while Fig. 1(b) presents the characteristic rounded grain shapes of different size fractions. The specific gravity is $G_s = 2.67$, and, according to ASTM D2487 (ASTM 2017), the field material classifies as well-graded gravel with sand (GW).

Particle shapes were measured in size fractions between 2 and 100 mm. Two characteristic shape descriptors were used: width-to-length sphericity (S_{WL} = particle width/particle length) and roundness [$R = \sum(r_i/N)/r_{in}$], where r_i represents the radius of circles fitted to concave corners of the particle, N is the number of the fitted circles, and r_{in} is the radius of the largest inscribed circle. Digital shape analyses were carried out on photos comprising more than 40 particles for each size fraction to ensure statistical representation. The detailed methodology followed for shape computations is found in the work of Zheng and Hryciw (2015). As shown in Fig. 1(c), R varies with particle size, covering a range from subrounded to well-rounded particles ($R = 0.3$–0.8). In contrast, S_{WL} remains relatively consistent across sizes, indicating medium to high sphericity ($S_{WL} = 0.6$–0.8).

Small-Scale Grading

Ten distinct PSDs were prepared from the original alluvial gravel: seven PSDs using the scalping grading method [Fig. 2(a)] and three PSDs using the truncation technique [Fig. 2(b)]. Grading was set based on the triaxial specimen diameter (D), in order to get a minimum specimen aspect ratio D/d_{max} of 8. Three triaxial devices were used, each accommodating different sizes: small specimens for $D = 100$ mm (hereafter referred to as S specimens), medium specimens with $D = 150$ mm (M specimens), and large specimens with $D = 800$ mm (L specimens); the apparatuses are available at the IBF laboratory of the Karlsruhe Institute of Technology (Brauns and Reith 2000; Brauns and Kast 2007). The materials having $d_{\text{max}} = 11$, 6.3, and 4 mm were tested as S specimens; $d_{\text{max}} = 20$, 11, and 6.3 mm as M specimens; and L specimens for the coarsest

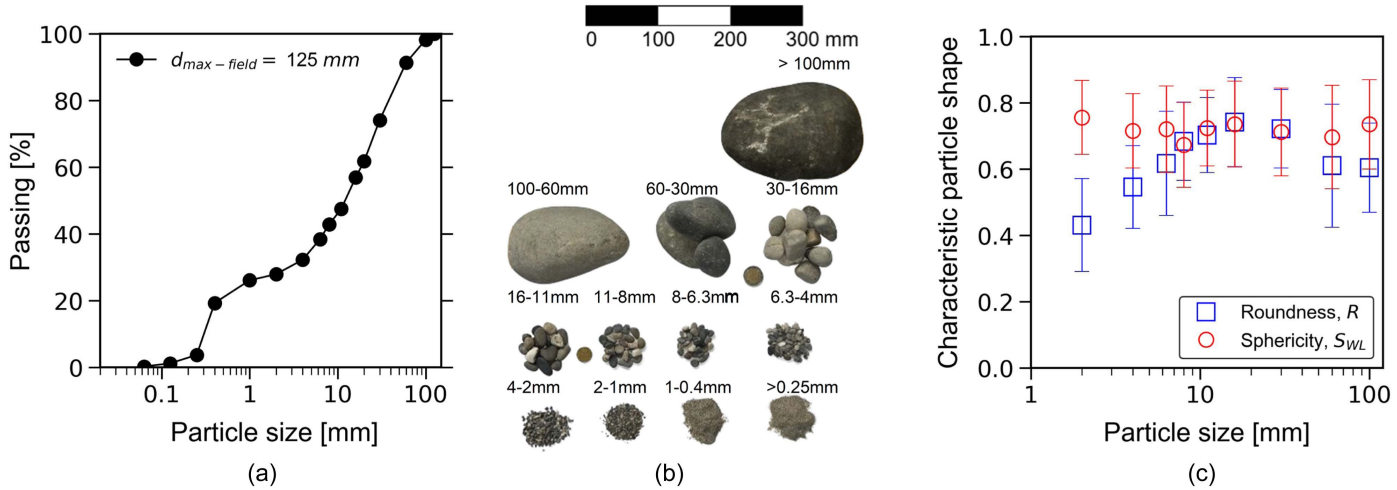

Fig. 1. Alluvial soil characterization: (a) PSD of the field soil; (b) photo of the particles; and (c) particle shapes over size fractions >1 mm.

J. Geotech. Geoenviron. Eng., 2026, 152(1): 04025166

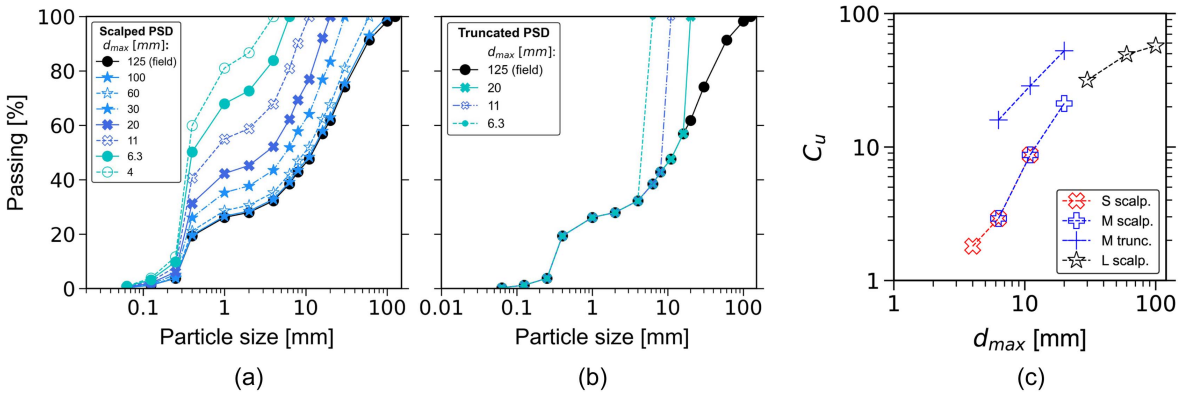

Fig. 2. Particle size distributions of the scaled materials from alluvial sandy gravel: (a) scalping grading; (b) truncation technique; and (c) evolution of C_u with $d_{\max}$ across all scaled specimens.

materials having $d_{\max} = 100$, 60, and 30 mm. The evolution of C_u ranging from 1.8 to 57.3 is plotted in Fig. 2(c), displaying a common trend of all the scalped materials and higher values for the truncated PSDs.

The determination of maximum ($\gamma_{d_{\max}}$) and minimum ($\gamma_{d_{\min}}$) dry densities was conducted according to the DIN 18126 (DIN 2022) standard for all the scalped PSDs having $d_{\max} \leq 60$ mm. Three mold diameters of $\varnothing = 250$, 150, and 100 mm were used based on the corresponding $d_{\max}$ of 60 and 30, 20 and 11, and 6.3 and 4 mm, respectively. To obtain $\gamma_{d_{\max}}$, dry specimens were placed in the molds with a scoop, gently enough to minimize particle rearrangement and densification. The mold was then fixed on the shaking table shown in Fig. 3(a), and a vertical spring load was applied to the specimen [see Fig. 3(b)]. The densest state was attained by vibrating the table at a frequency of 1.66 ± 0.1 Hz for 5 min. Each PSD was tested three times using virgin material. After each trial, three separate settlement values were recorded, cumulating nine distinct measurements for each PSD. Finally, the mean values were used to obtain $\gamma_{d_{\max}}$.

The materials used for $\gamma_{d_{\max}}$ determination were subsequently reused to obtain $\gamma_{d_{\min}}$, in order to account for any potential degradation of the particles. For specimens tested with $\varnothing = 250$ and 150 mm molds, the loosest configuration was achieved by gently placing dry material into the mold using a scoop. For specimens tested with the $\varnothing = 100$ mm mold, a funnel was used instead of the scoop [see Fig. 3(c)]. The funnel was positioned by the bottom of the mold, and the material was gradually poured. Six separate trials were repeated for each PSD sample. $\gamma_{d_{\min}}$ was then calculated using the mean values. The values of $\gamma_{d_{\max}}$ and $\gamma_{d_{\min}}$ of each PSD are plotted in Fig. 4(a). The results show increasing density with C_u (i.e., increasing $d_{\max}$), with better graded specimens reaching denser packings. The corresponding maximum ($e_{\max}$) and minimum ($e_{\min}$) void ratios were subsequently calculated, and the density index (I_D) was obtained as

$$I_D = \frac{e_{\max} - e}{e_{\max} - e_{\min}}$$

As proposed by Biarez and Hicher (1997) and displayed in Fig. 4(b), $e_{\max}$ and $e_{\min}$ correlate with particle roundness, showing relatively stable values beyond $C_u \geq 10$.

Triaxial Testing Program

A detailed summary of 21 tests is listed in Table 1, showing six S specimens, nine M specimens, and six L specimens. All specimens have a height-to-diameter ratio of $H/D = 1$ and lubricated end platens to minimize heterogeneous strain fields. The tests involved

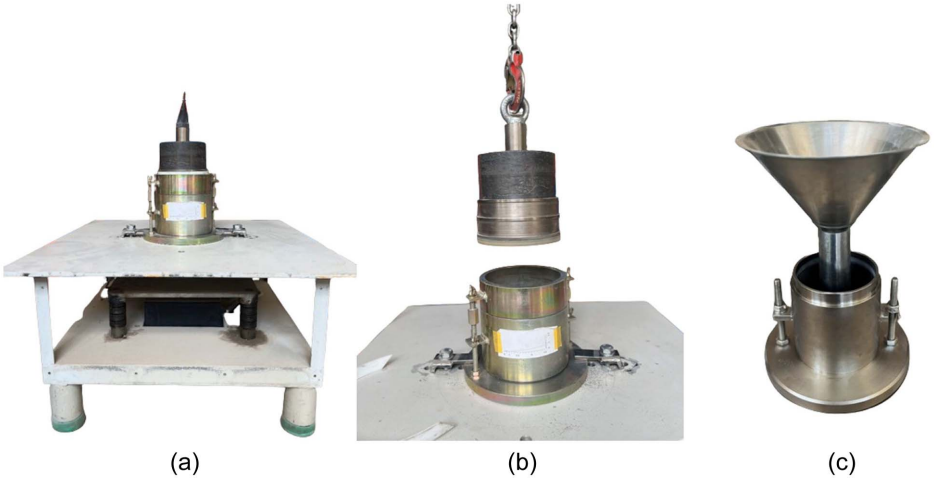

Fig. 3. Experimental setup for maximum and minimum densities: (a) shaking table for $\gamma_{d_{\max}}$ determination; (b) spring load showcase for $\varnothing = 150$ mm mold; and (c) $\gamma_{d_{\min}}$ determination setup for specimens with $d_{\max} \leq 6.3$ mm.

J. Geotech. Geoenviron. Eng., 2026, 152(1): 04025166

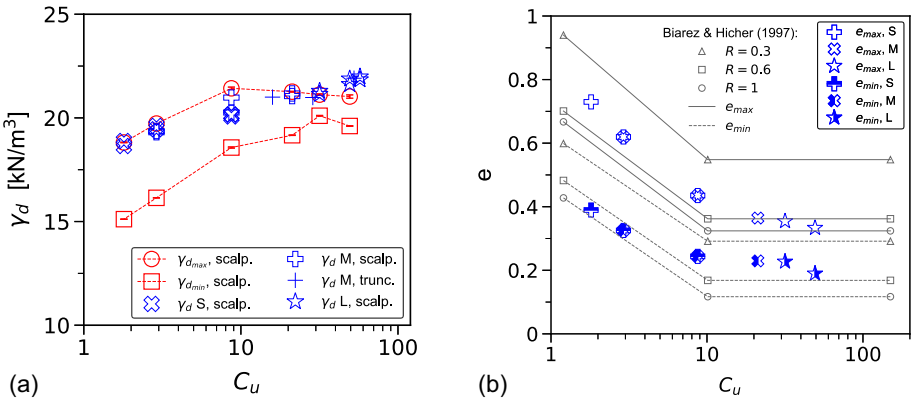

Fig. 4. Packing properties for all scaled materials: (a) $\gamma_{d_{max}}$ and $\gamma_{d_{min}}$ (mean from nine distinct values for $\gamma_{d_{max}}$ and six values for $\gamma_{d_{min}}$); and (b) comparison with the correlations of Biarez and Hicher (1997).

Table 1. Summary of the triaxial tests performed

Specimen ID	D (mm)	Scaling	d_{max} (mm)	C_u	γ_d (kN/m^3)	e	σ_3' (kPa)	B	E_{50} (MPa)	ϕ_p' (degrees)	ϕ_{cr}' (degrees)	ψ_{max} (degrees)	e_{cr}[a]
S1	100	Scalping	4	1.8	18.64	0.43	100	0.98	56.2	47.0	39.2	21.0	0.57
S2	100	Scalping	6.3	2.9	19.45	0.37	100	0.98	60.2	46.5	38.5	21.4	0.50
S3	100	Scalping	11	8.7	20.15	0.32	100	0.98	61.9	48.6	40.3	21.1	0.42
S4	100	Scalping	4	1.8	18.88	0.41	600	0.99	199.2	42.9	37.1	12.6	0.48
S5	100	Scalping	6.3	2.9	19.61	0.36	600	0.95	180.7	42.8	38.0	11.9	0.41
S6	100	Scalping	11	8.7	20.17	0.32	600	0.98	149.0	44.1	40.0	10.7	0.35
M1	150	Truncation	6.3	2.9	19.31	0.38	100	0.98	63.7	48.5	40.6	20.0	0.48
M2	150	Truncation	11	8.7	20.26	0.32	100	0.98	56.8	48.8	41.7	19.8	0.36
M3	150	Truncation	20	21.2	21.18	0.26	100	0.96	83.7	49.6	40.1	21.1	0.33
M4	150	Truncation	6.3	2.9	19.37	0.38	600	0.98	163.1	42.6	36.8	12.2	0.43
M5	150	Truncation	11	8.7	20.98	0.27	600	0.85	187.1	43.5	38.4	11.6	0.30
M6	150	Truncation	20	21.2	21.05	0.27	600	0.98	191.0	44.0	38.9	11.1	0.29
M7	150	Truncation	6.3	15.9	21.00	0.27	100	0.99	45.9	47.3	42.9	19.7	0.33
M8	150	Truncation	11	28.7	20.98	0.27	100	0.99	68.0	49.0	42.0	18.1	0.34
M9	150	Truncation	20	52.5	21.91	0.22	100	0.99	77.5	50.4	42.6	16.2	0.26
L1	800	Scalping	30	31.7	21.29	0.25	100	—	80.4	50.0	44.9	14.2	0.28
L2	800	Scalping	60	49.3	21.62	0.23	100	—	92.8	47.6	44.9	11.9	0.24
L3	800	Scalping	100	57.3	21.98	0.21	100	—	58.3	49.4	46.6	13.2	0.23
L4	800	Scalping	30	31.7	21.15	0.26	600	—	263.1	45.5	42.4	8.4	0.27
L5	800	Scalping	60	49.3	21.89	0.22	600	—	206.6	46.3	41.8	8.8	0.23
L6	800	Scalping	100	57.3	21.85	0.22	600	—	228.0	44.6	42.1	9.9	0.22

[a]Estimated critical state values.

monotonic triaxials on saturated dense specimens under consolidated drained conditions.

- S specimens, D = 100 mm

  As indicated in Table 1, all S specimens were prepared using scalped materials. End platens were lubricated using silicon grease, as displayed in Fig. 5(a). Specimens were prepared at a dense state by mounting six distinct layers of homogeneous dry material, each one with a mass around ~285g, and compacted using standard Proctor hammer blows to attain a targeted thickness. Due to the different PSDs, the γ_d for each specimen varied slightly between 18.64 and 20.15 kN/m^3, as displayed in Fig. 4(a) and Table 1. However, I_D remained above 0.9 for all specimens.

  After flushing the specimen with CO_2 and deaired water for a minimum of 1 h, saturation started by gradually raising the back pressure (σ_{cp}). After 24 h, the Skempton coefficient ($B = \delta u/\delta\sigma_3$, where u is the pore pressure) was checked, and a specimen was deemed fully saturated when $B \geq 0.95$ (see Table 1).

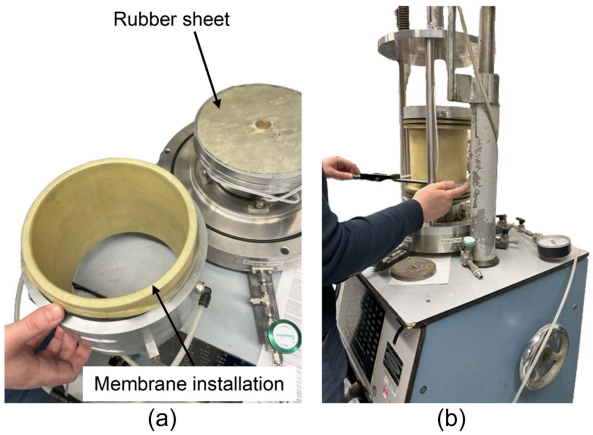

Fig. 5. S and M tests setup: (a) test base preparation; and (b) specimen dimension measurements.

Isotropic consolidation started by maintaining a desired effective confining stress ($\sigma_3' = \sigma_3 - \sigma_{cp}$), until the volumetric strain (ε_v) had stabilized. Two σ_3' of 100 and 600 kPa were considered in this study. Lastly, the shear stage was performed at constant vertical displacement rate of 0.10 mm/min, and the deviatoric stress ($q = \sigma_1' - \sigma_3'$) was monitored until an axial deformation (ε_a) of 24%.

- M specimens, D = 150 mm

A similar protocol described previously for S specimens was followed for M specimens. For comparison, six tests were accommodated using materials prepared with the scalping grading method, and three by the truncation technique (see Table 1); $\sigma_3' = 100$ and 600 kPa were used for scalped specimens ($C_u = 2.9$–21), and only $\sigma_3' = 100$ kPa was considered on truncated specimens having $C_u = 15.9$–46. Dense M specimens were mounted in eight dry homogeneous layers and compacted using a standard Proctor hammer. Each layer had a mass of ~675g and ~725 g for scalped and truncated specimens, respectively. Due to diverse C_u values of the tested materials, the attained γ_d varied between 19.31 and 21.18 kN/m^3 for scalping and 20.98 and 21.91 kN/m^3 for truncation [see Fig. 4(a)]; $I_D \geq 0.9$ was also achieved in all M cases. Following the same procedure as S specimens, the saturation stage proceeded and M specimens were deemed fully saturated when $B \geq 0.95$, usually after 48 to 72 h. Specimens were then consolidated at a targeted σ_3' and sheared at a constant rate of ~0.14 mm/min up to $\varepsilon_a = 24\%$.

- L specimens, D = 800 mm

Fig. 6 illustrates the triaxial test setup for L specimens. Six materials with C_u between 32 and 57 were scalped and tested at $\sigma_3' = 100$ and 600 kPa. The total mass of L specimens was approximately 900 kg. The base was lubricated with silicon grease and a rubber sheet was added [see Fig. 6(a)]. A 5 mm thick membrane was then installed in the mold [Fig. 6(b)], as well as metal plates to protect it from puncturing during compaction [Fig. 6(c)]. A thin sand layer was added to improve the saturation through the porous stone [Fig. 6(c)]. Dense specimens were

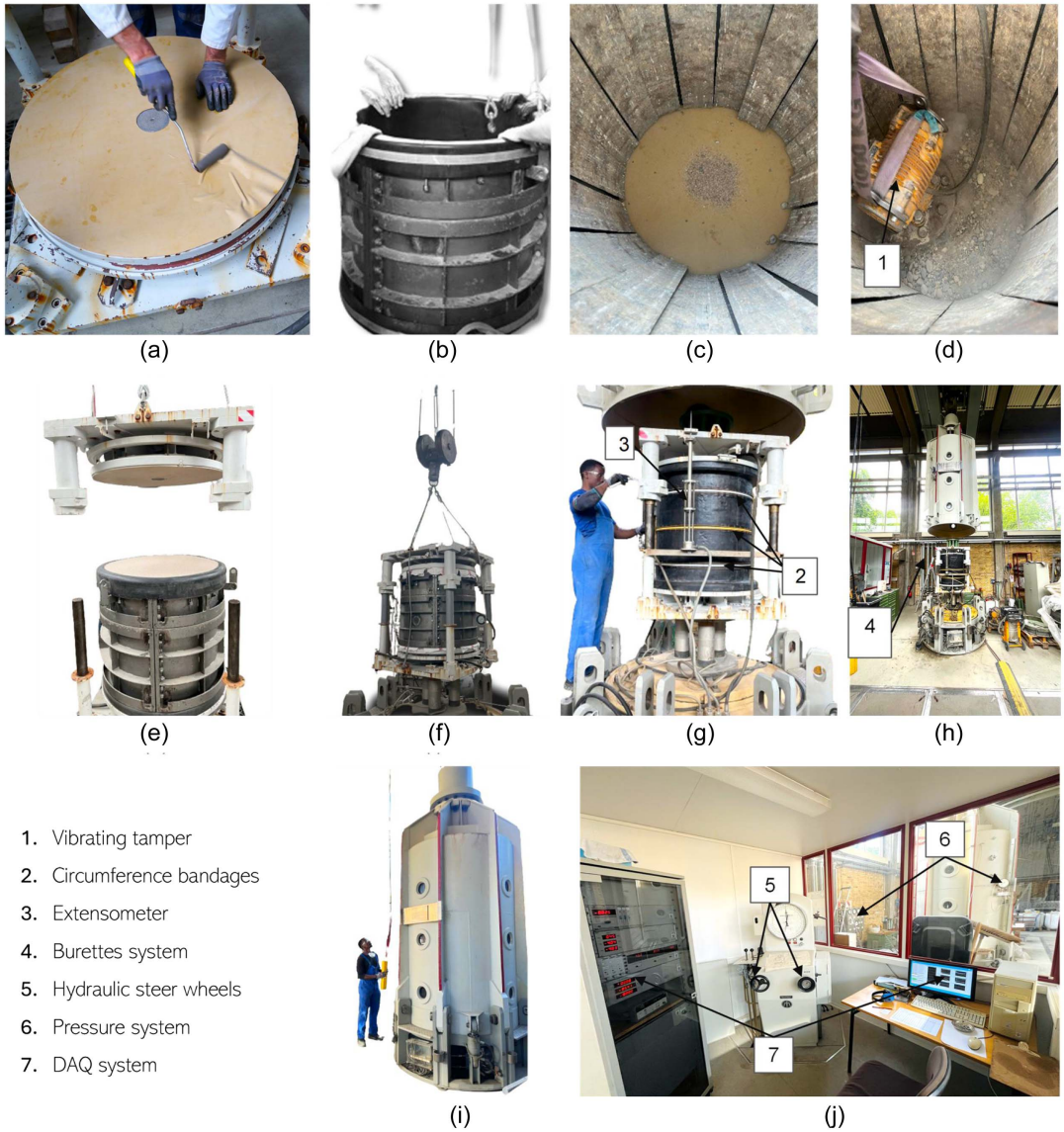

Fig. 6. Setup of L specimens: (a) adding rubber to the lubricated base platen; (b) membrane installation; (c) installing membrane protection plates and sand layer at the center to protect drainage; (d) filling the material inside and compacting; (e) adding a sand layer to level the top surface; (f) specimen transportation to the testing pedestal; (g) placing circumference bandages and vertical displacement extensometers; (h) installing the cell; (i) specimen ready for testing; and (j) data acquisition system.

J. Geotech. Geoenviron. Eng., 2026, 152(1): 04025166

prepared using eight homogeneous layers of dry material, each weighing around ~110 kg. Compaction was done layer by layer using a vibrating tamper [see Fig. 6(d)] until a thickness of 10 cm was reached. This approach was selected to achieve uniform densification primarily through particle rearrangement, while minimizing particle fragmentation during preparation. Before adding subsequent layers, the top surface was scratched to ensure contact homogeneity. At the mid-height (before adding the fifth layer), density was checked to verify whether the specimen respected the targeted γ_d. In the case of noncompliance, the mold containing the four layers was transported to the triaxial device pedestal to apply static compaction using the built-in hydraulic jack. Then, it was returned for the completion of the remaining layers. After the material was filled, the metal plates were removed from the mold.

In all L specimens, the attained γ_d varied between 21.15 and 21.98 kN/m^3. Thus, $I_D \geq 0.9$ was achieved in materials having $d_{\max} = 30$ and 60 mm, as in S and M specimens. After the results shown in Fig. 4(a), it is assumed that PSDs with $d_{\max} = 100$ mm reached similar I_D, since equivalent particle shapes are involved and the same compaction method was used. A 2 cm thick layer of sand was added on top of the last layer to level the top surface and prevent imperfections [see Fig. 6(e)]. As shown in Fig. 6(f), the specimen was then transferred to the testing pedestal, where the mold was removed after applying vacuum (~90 kPa) to hold the specimen. Initial measurements of the specimen height at three positions were taken, as well as specimen diameters at the top, middle, and bottom levels. Also, circumference bandages were added on the top, middle, and bottom of the specimen to track radial strain measurements (ε_r) during isotropic consolidation and shearing. In addition, three vertical displacement extensometers were positioned for ε_a measurements [Fig. 6(g)].

Fig. 6(h) presents the installation of the cell, with a built-in hydraulic system that allows the cell to close properly and apply deviatoric stress; the final installation step is shown in Fig. 6(i). Finally, the cell was filled with water for about 2 h. Upon completion, the vacuum was gradually removed, while simultaneously applying a cell pressure of 100 kPa to hold the specimen. The saturation step was followed by filling water during 24 h inside the specimen, from bottom to top using a burette system.

In contrast with S and M specimens, where the B value check was used to assess the saturation degree, "full saturation" was assumed for L specimens when water flew out from the specimen via a clear vinyl hose that had been attached for this end. The uncertainty in the B value for the L specimens could not be resolved experimentally. However, this is expected to have a minimal influence on the results of the drained triaxial tests, since the volumetric strain is measured using local bandages [refer to Fig. 6(g)], which are not affected by the volumetric changes in the gas (air) that would influence a global measurement. Additionally, the drained nature of the tests prevents the generation of excess pore water pressure, further minimizing the impact of this uncertainty. L specimens were subsequently consolidated at the desired σ_3', after which shearing proceeded "manually" at a constant rate of 0.4 mm/min (0.05%/min) using the hydraulic steering wheels shown in Fig. 6(j). This shear rate was adopted as a precaution to account for the uncertainty of full saturation condition in these samples, allowing pore water pressure dissipation. The data acquisition system involved a computer that recorded automatically and continuously the applied q, ε_a (through vertical extensometer readings), and σ_3' from the pressure sensor [see Fig. 6(j)]. The readings from the circumference bandages were done manually every 5 min, and data were updated in the computer until $\varepsilon_a \sim 15\%$ was reached (around 5 h).

Results

Stress–strain responses in terms of the stress ratio q/p' [p' being the mean effective stress given by $p' = (\sigma_1' + 2\sigma_3')/3$] are plotted against ε_a for all the materials tested; S, M, and L specimens are displayed in Figs. 7–9, respectively. Continuous lines designate scalped specimens, and dashed or pointed lines indicate truncated specimens. Strain relationships represented by the volumetric strain (ε_v) plotted against ε_a are equally shown in the same figures. It is noteworthy to recall that ε_v was measured directly from drained water during shearing in S and M specimens, while ε_v in L specimens was estimated from ε_r readings as

$$\varepsilon_v = 1 - (1 - \varepsilon_a)(1 - \varepsilon_r)^2$$

All tests showed hardening and peak q/p' values, which were recorded around $\varepsilon_a = 3\%$ and 6% for $\sigma_3' = 100$ and 600 kPa, respectively. A softening regime followed after peak, converging toward ultimate q/p' values at large strains beyond $\varepsilon_a \geq 13\%$. As expected, the peak shear strength and dilatancy decrease with σ_3'. Normalized shear strength q/p' at large strains tends to similar values for a given specimen size, which is expected since the specimens have equivalent relative densities and the same characteristic particle shape. All specimens displayed dilatant behavior as early as $\varepsilon_a \sim 1\%$ for $\sigma_3' = 100$ kPa and $\varepsilon_a \sim 3\%$ for $\sigma_3' = 600$ kPa. Interestingly, in all the cases volumetric dilatancy decreases with increasing C_u, which is a well reported observation in the literature (Muir Wood and Maeda 2008; Yang and Luo 2018; Ahmed et al. 2023). The maximum ε_v attained on scalped specimens varied with size and σ_3'; on average, $\varepsilon_v \sim -11\%$, -8%, and -3% at $\sigma_3' = 100$ kPa, and $\varepsilon_v \sim -5\%$, -5%, and -3% at $\sigma_3' = 600$ kPa, for S, M, and L specimens, respectively.

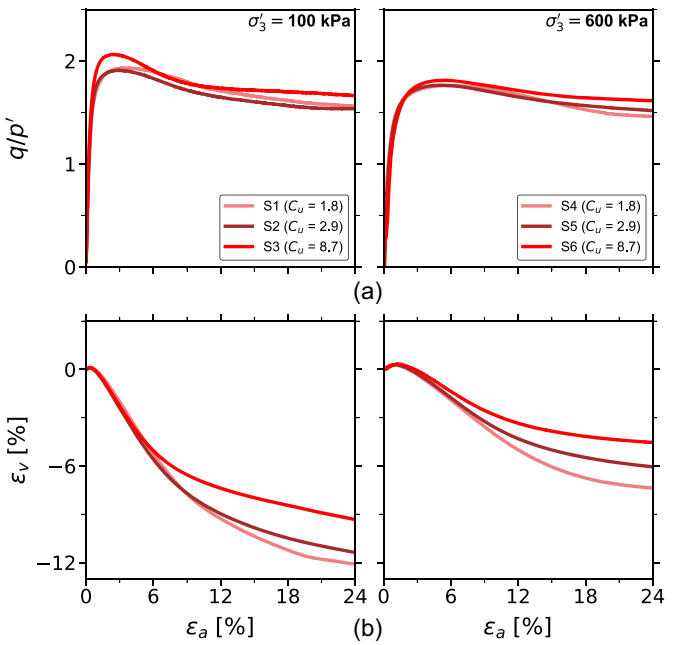

Fig. 7. Stress strain curves of S specimens: (a) q/p' versus ε_a; and (b) ε_v versus ε_a.

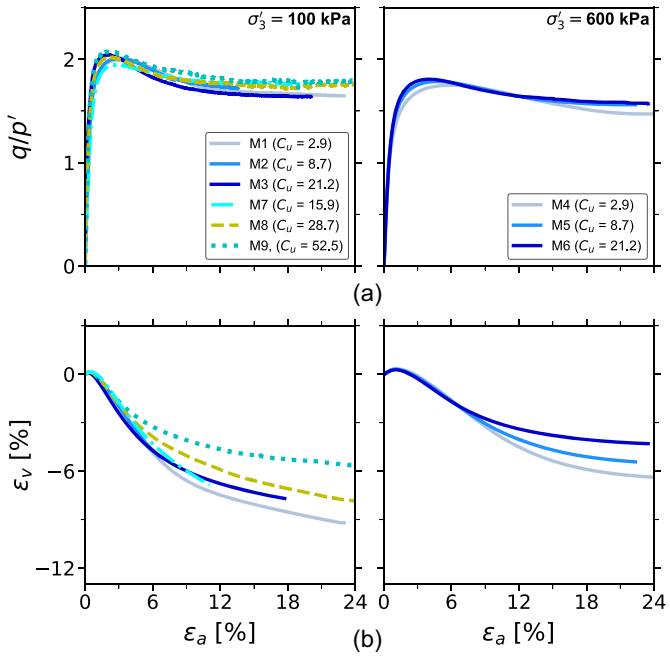

Fig. 8. Stress strain curves of M specimens: (a) q/p' versus ε_a; and (b) ε_v versus ε_a.

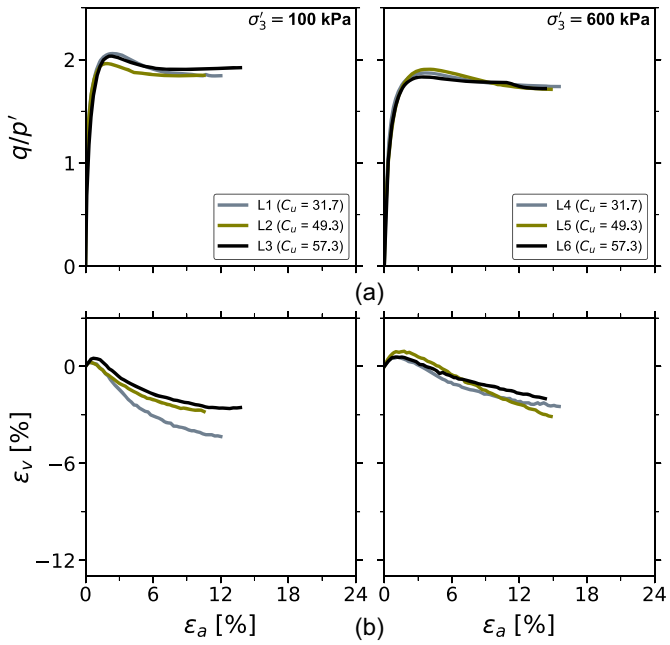

Fig. 9. Stress strain curves of L specimens: (a) q/p' versus ε_a; and (b) ε_v versus ε_a.

Selected S and M specimens were sieved after testing to compare the amounts of particle breakage at $\sigma_3' = 600$ kPa. Fig. 10 shows that changes in PSD after testing are mostly not significant and particularly negligible in size fractions coarser than 1 mm. Moreover, the masses of the finest fractions increased in less than 5%. In order to properly quantify such low amounts of particle breakage, three different breakage indexes were used. The index introduced by Marsal (1967), denoted as B_g, primarily reflects

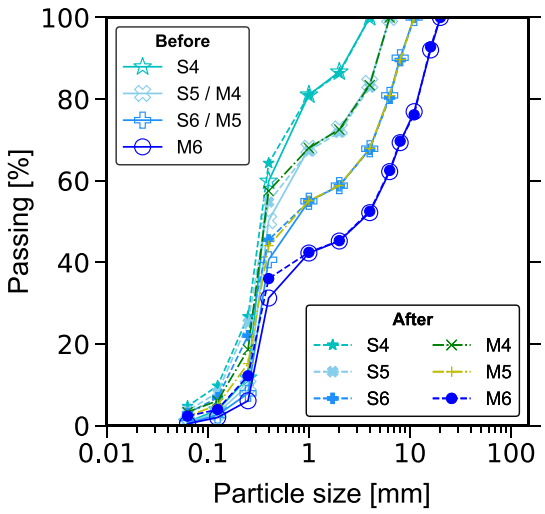

Fig. 10. Initial and final PSD comparison for particle breakage quantification.

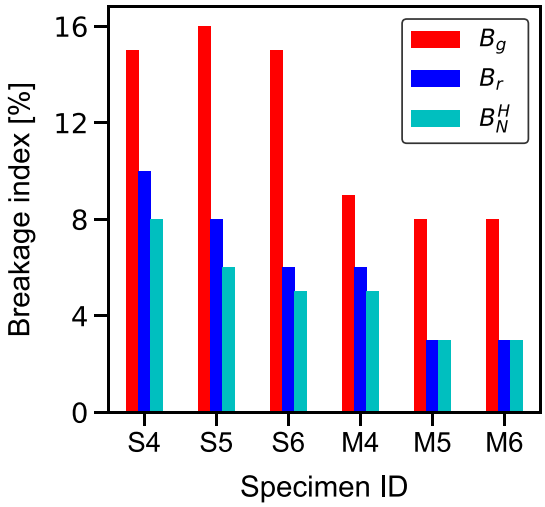

Fig. 11. Comparison between breakage indexes of S and M specimens tested at $\sigma_3' = 600$ kPa.

the reduction in coarse fractions by summing only the positive increments (before and after a test) of retained mass percentages over all size fractions. In contrast, the index B_r, proposed by Hardin (1985), evaluates the ratio of the actual amount of breakage to the ultimate breakage, which is assumed to be reached once 100% of the particles are finer than 74 μm. Specifically, B_r is defined as the area between the PSDs before and after testing, divided by the area between the initial and the ultimate PSD. According to Xiao et al. (2021), B_g overlooks total breakage due to its focus on coarse fractions, while B_r is sensitive to the number of size intervals. To address these limitations, Xiao et al. (2021) proposed the normalized breakage index $B_N^H = (M^c - M^i)/(M^u - M^i)$, where M^i, M^c, and M^u represent the sum of the cumulative passing-sieve mass percentages over each size fraction in the initial, final, and ultimate PSDs, respectively; H refers to the Hardin-based formulation, which defines the ultimate PSD. Fig. 11 compares the three indexes for S and M specimens tested at $\sigma_3' = 600$ kPa. It is worth noting that B_r and B_N^H represent global breakage across all sieve fractions,

while B_g specifically quantifies the loss of mass from the coarser retained fractions; this distinction explains why B_g consistently indicates higher values compared to B_r and B_N^H. All indexes corroborate that S specimens experienced greater particle breakage than M specimens, most probably due to differences in characteristic particle shape. Additionally, scale effects in PSD led to a shift in soil classification from GW to GP (poorly graded gravels) in the smaller specimens, thereby increasing their susceptibility to breakage.

Analysis and Discussion

Dilatancy

The maximum dilatancy angle ($\psi_{\max}$) mobilized is defined as (Schanz and Vermeer 1996)

$$\sin\psi_{\max} = \frac{-(d\varepsilon_v/d\varepsilon_a)_p}{2-(d\varepsilon_v/d\varepsilon_a)_p}$$

where $(d\varepsilon_v/d\varepsilon_a)_p$ = dilatancy ratio at the peak deviatoric stress; $\psi_{\max}$ is plotted in Fig. 12 against C_u for all the tests carried out. Results are arranged for each σ_3' and specimen size with distinct colors and markers. On average, $\psi_{\max}$ mobilized was 21.1°, 20.3°, and 13.1° at $\sigma_3' = 100$ kPa and 11.7°, 11.6°, and 8.8° at $\sigma_3' = 600$ kPa on S, M, and L scalped specimens, respectively. It can be observed that $\psi_{\max}$ values remain relatively consistent across S and M scalped specimens, which share the same soil classification as poorly graded (GP). In contrast, L scalped specimens and M truncated specimens—classified as GW—exhibit lower $\psi_{\max}$ values. This trend is particularly pronounced and more scattered at lower confining pressure (i.e., $\sigma_3' = 100$ kPa).

These findings are consistent with previously cited studies indicating that, under a given shearing stress path and relative density, volumetric dilatancy decreases with grain size polydispersity (Yan and Dong 2011; Amirpour Harehdasht et al. 2017; Yang and Luo 2018; Cantor et al. 2018; Deng et al. 2021; Ahmed et al. 2023; Zhang et al. 2024). This is because more diverse pore sizes allow for more efficient packing, enabling easier rearrangement and filling with varying grain sizes. Conversely, a relatively large volume of similar-sized pores in uniformly graded soils leads to high volume changes upon dilation. Therefore, since small-scale techniques generate specimens that are more uniformly graded than the original coarse soil, it is important to recognize that the volumetric deformation might be overestimated in geotechnical designs.

Secant Strain Modulus

The characteristic stiffness of the specimens was analyzed based on E_{50}, defined as the secant strain modulus at 50% of the peak deviatoric stress ($q_{\max}$)

$$E_{50} = \frac{0.5q_{\max}}{\varepsilon_{a-q_{\max}}}$$

Fig. 13 presents E_{50} against C_u for all the tests in this study. Combining all the C_u values for each specimen size, the average modulus of scalped specimens is around $E_{50} = 59$, 68 and 77 MPa for $\sigma_3' = 100$ kPa and $E_{50} = 76$, 180 and 233 MPa at 600 kPa on the S, M, and L specimens, respectively. This suggests that for all σ_3' used, L specimens exhibit around 15% to 30% higher strain moduli compared to S and M specimens. Therefore, small-scaling results in conservative stiffness values compared to the coarser material stiffness. While this behavior might appear to contradict the dilatancy trend, it is vital to recognize that these two parameters reflect distinct aspects of soil behavior. As previously stated, well-graded specimens comprise more efficient packing, which enhances interparticle contact and initial stiffness despite the reduced potential for volumetric dilation. In contrast, uniformly graded soils mobilize lower peak strength and greater volumetric deformation, due to the larger void space prevalent. Moreover, the lower stiffness values in S specimens might also be attributable to the increased extent of particle breakage, as previously shown in Fig. 11.

A comparison of E_{50} with data of coarse rockfills ($d_{\max} =$ 100–200 mm, from blasted and quarried rocks) compiled in Ovalle et al. (2020) is presented in Fig. 14. Empirical relationships for quartz sands proposed by Schanz and Vermeer (1998) are also included. One can observe that the tested alluvial gravels exhibited much higher E_{50} than coarse rockfills, aligning with reported data on diverse gravel materials from several authors (Verdugo and de la Hoz 2007; Liu et al. 2016; Wang et al. 2022). This is mainly due to enhanced particle crushing of highly angular rock grains and relatively weak crushed rock particles resulting from blasting. On the other hand, alluvial and fluvial gravels are typically composed of strong eroded particles.

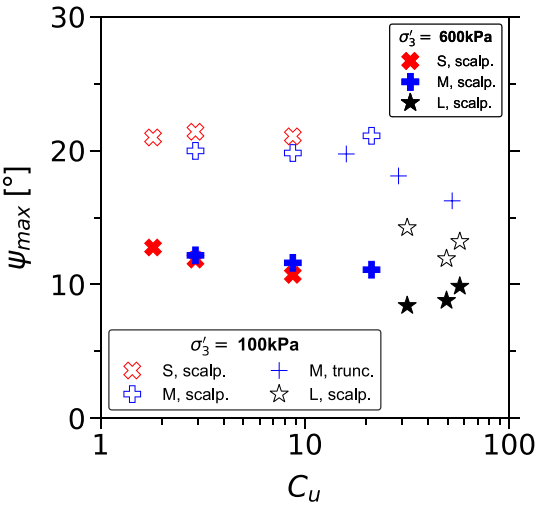

Fig. 12. Dilatancy angle $\psi_{\max}$ against C_u for all specimens.

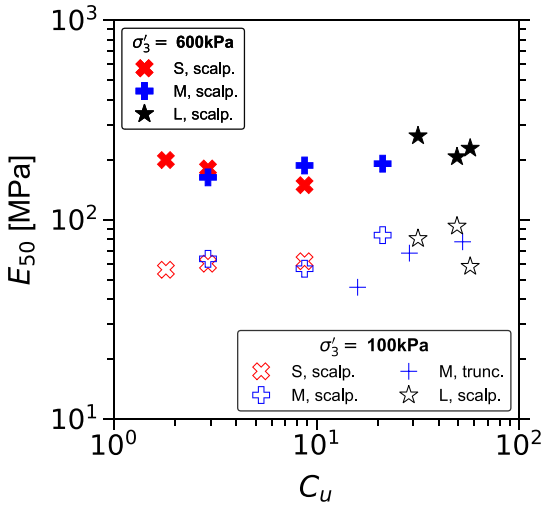

Fig. 13. Secant strain modulus E_{50} against C_u for all specimens.

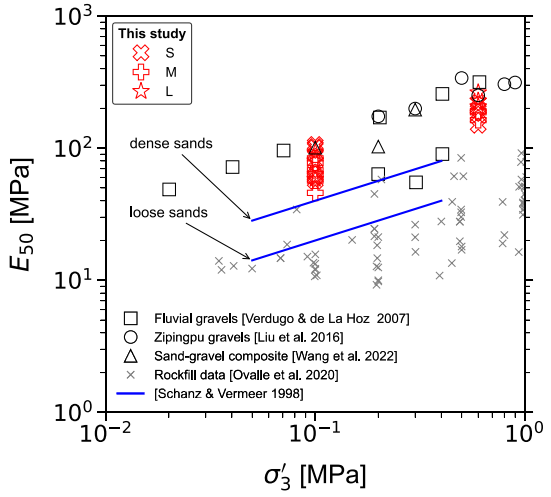

Fig. 14. Comparison of E_{50} with reported triaxial data on rockfill and gravel materials, as a function of σ'_3.

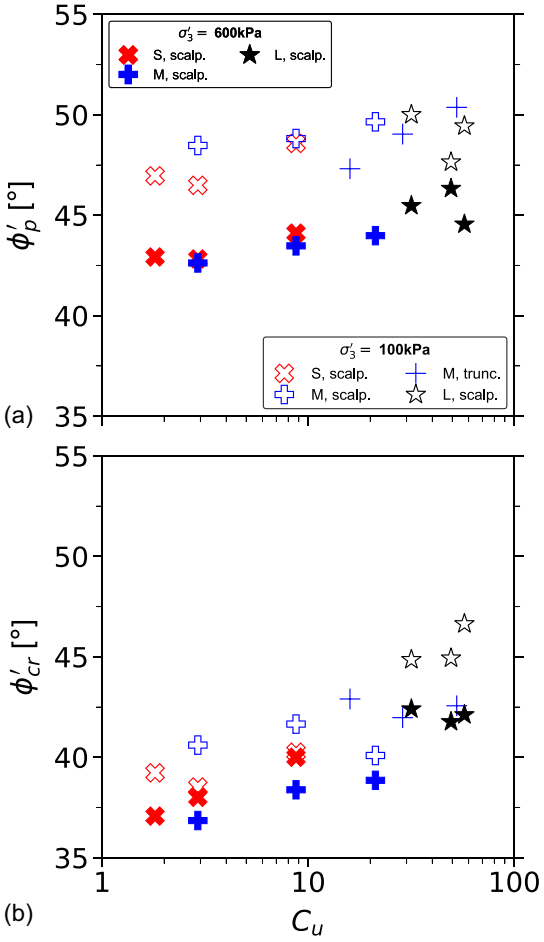

Fig. 15. Specimen size and grading effects on effective friction angles: (a) ϕ'_p versus C_u; and (b) ϕ'_{cr} versus C_u.

Shear Strength

The shear strength was assessed as the mobilized effective friction angle (ϕ'), estimated according to the Mohr–Coulomb failure criterion for noncohesive materials

$$\sin\phi' = \frac{3M}{6+M}$$

where $M = q/p'$ at the maximum strength for the peak friction angle (ϕ'_p) and at the steady state for the critical friction angle (ϕ'_{cr}). The dilatant dense specimens did not fully reach critical state, particularly in terms of volumetric strains. However, ϕ'_{cr} was assumed to mobilize at the largest vertical strain in each test, since the results in terms of q/p' are reasonably stable after $\varepsilon_a = 12\%$. For all the scalped specimens at $\sigma'_3 = 100$ kPa, Fig. 15 shows that ϕ'_p varied between 46.5° and 50.0°. For different specimen sizes, the average $\phi_{p'}$ varied in the order S < M ≈ L, with less than 2° of dispersion around the mean value. Similar observations are found at $\sigma'_3 = 600$ kPa, with ϕ'_p ranging between 43.3° and 45.5° and the average values in the order S ≈ M < L. In other words, within the scope of the investigated grading methods and specimen sizes, the tested alluvial gravels presented a slight size effect on ϕ'_p, where the small-scale specimens exhibit lower strength values than coarser materials.

Fig. 15 also shows that ϕ'_{cr} has remarkable variations across the specimens sizes and C_u, with averages values of around 39.3°, 40.8°, and 45.5° at $\sigma'_3 = 100$ kPa and 38.4°, 38°, and 42.1° at $\sigma'_3 = 600$ kPa for the S, M, and L specimens, respectively. In addition to the reasoning provided previously, several other causes for such results are presumed: (1) the particle shape-size correlation shown in Fig. 1(c) could strongly affect ϕ'_{cr}, as reported by Ovalle and Dano (2020) after large triaxial tests and by Carrasco et al. (2023) using DEM simulations; (2) specimens did not fully attain the critical state conditions at the reached ε_a levels; and (3) the strain fields of the specimens at postpeak states might have impacted the mobilized stresses due to localized deformations. Indeed, as presented in Fig. 16, a visual inspection of photos taken at the end of each test attests different deformation modes, particularly some specimens experiencing overexpansion at the top or at the bottom section. The observed heterogeneous strain fields suggest that end restraint effects are not overcome by using lubricated plates in such strong soils. The high frictional stresses mobilized by coarse soils might require increased slenderness to avoid this effect. Consequently, in this case the critical state strength can only be considered as an estimated value.

Excess friction angle, defined as $\phi'_p - \phi'_{cr}$, was correlated with ψ_{max} and compared with the expression proposed by Bolton (1986)

$$\phi'_p = \phi'_{cr} + K\psi_{max}$$

where K = empirical parameter for a given soil (i.e., constant C_u). Fig. 17 shows that $K = 0.48$, proposed by Bolton for uniform dense sands, overestimates the well graded alluvial gravels presented here (M and L). Also, data on gravel materials from the literature (Xiao et al. 2014, 2016; Strahler et al. 2016) are included for comparison, showing that the results of this study are within reported values of $K = 0.21$ to 0.58.

Critical State

Fig. 18 presents the stress deformation path in the $e - p'$ space for all the tests carried out in this study. Although steady states were not reached completely in the tests, the critical state lines (CSLs) were drawn simply by estimating the critical void ratios (e_{cr}) at the largest deformation reached in each test, in order to perform a comparative analysis. In the set of three plots presented in Fig. 18, C_u for a given specimen size (S, M, or L) decreases from left to right. As a consequence, the volumetric dilatancy increases significantly, particularly in S specimens (red markers in Fig. 18). The same

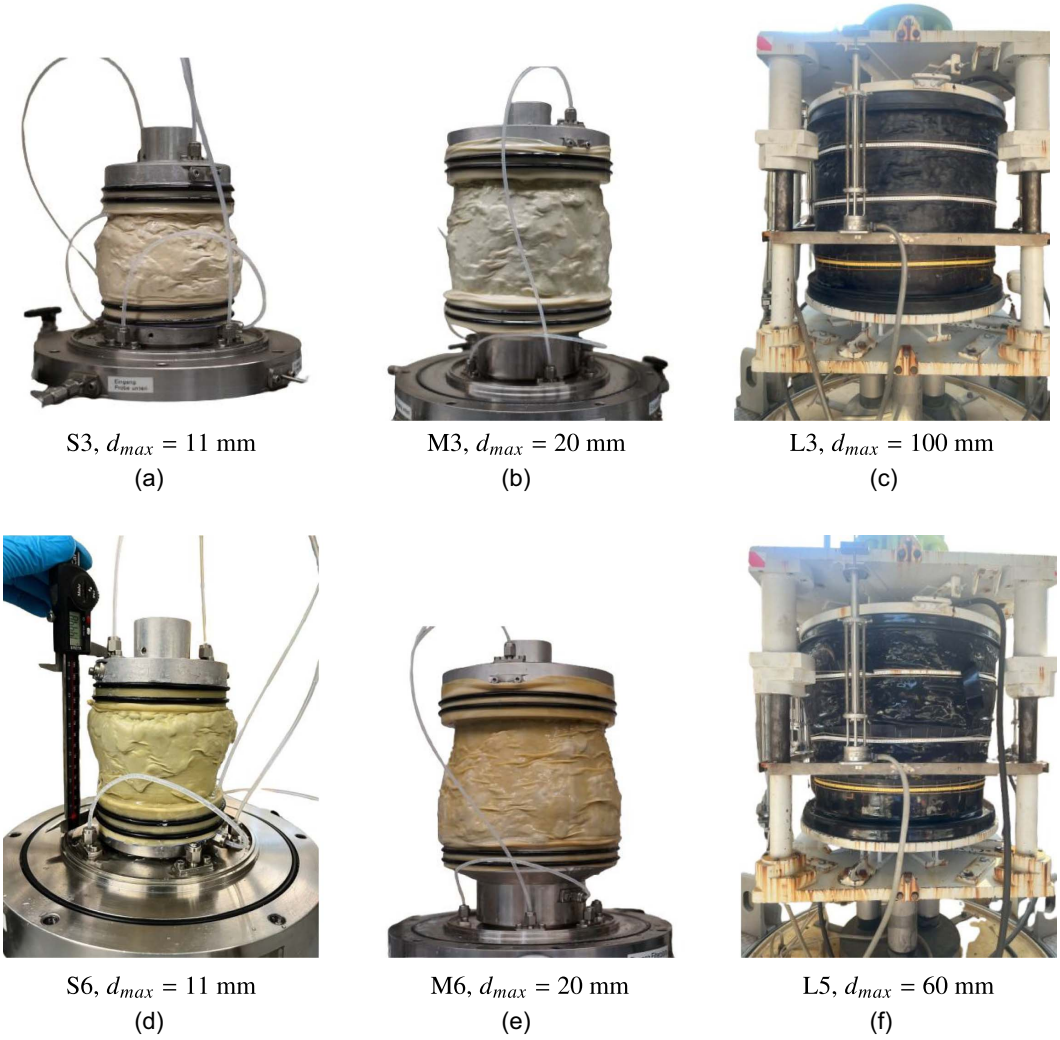

Fig. 16. Specimens after tests: (a and d) S specimen; (b and e) M specimen; and (c and f) L specimen. Panels (a)–(c) show $\sigma_3' = 100$ kPa, and panels (d)–(f) show $\sigma_3' = 600$ kPa.

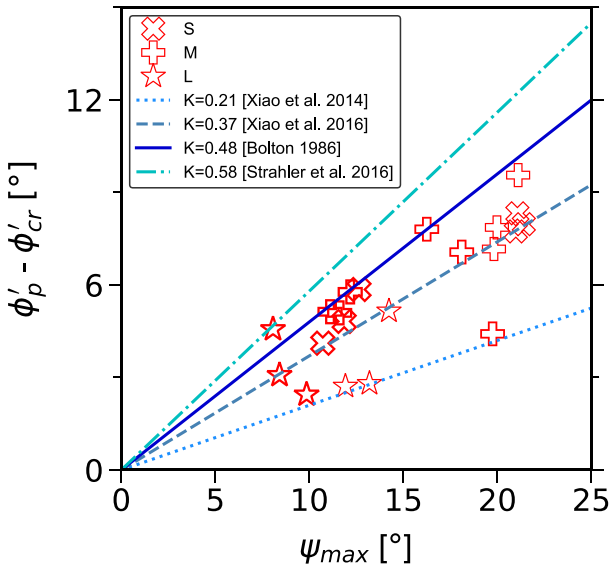

Fig. 17. Comparison of the excess friction angle with reported values in gravels.

tendency is observed within a single plot showing different specimen sizes; i.e., the lower the C_u, the higher e_{cr} and the volumetric dilatancy. This is also shown in Figs. 7–9 in terms of volumetric strains. As a result, the CSL is dragged down in the volume–stress space once C_u increases, consistently with the well-known PSD effects on critical state. Also, the slope of the CSL evolves, which might be affected by diverse properties, such as initial density, particle shape varying across grain sizes, and heterogeneous strain fields at large strains. To highlight the evolution of the critical state with grading, Fig. 19 shows e_{cr} as a function of C_u for all tests, where the values distinctly decrease as the materials become better graded. Two fitted power laws correspond to the sets of tests at different confining pressures $\sigma_3' = 100$ and 600 kPa, which closely match the experimental data.

Conclusions

In order to assess the impacts of small-scaling and grading on the mechanical behavior of coarse soil, 21 monotonic triaxial tests were carried out on dense alluvial gravel materials under consolidated drained conditions. A field soil with a maximum grain size of 125 mm was sampled, and small-scale specimens were prepared

J. Geotech. Geoenviron. Eng., 2026, 152(1): 04025166

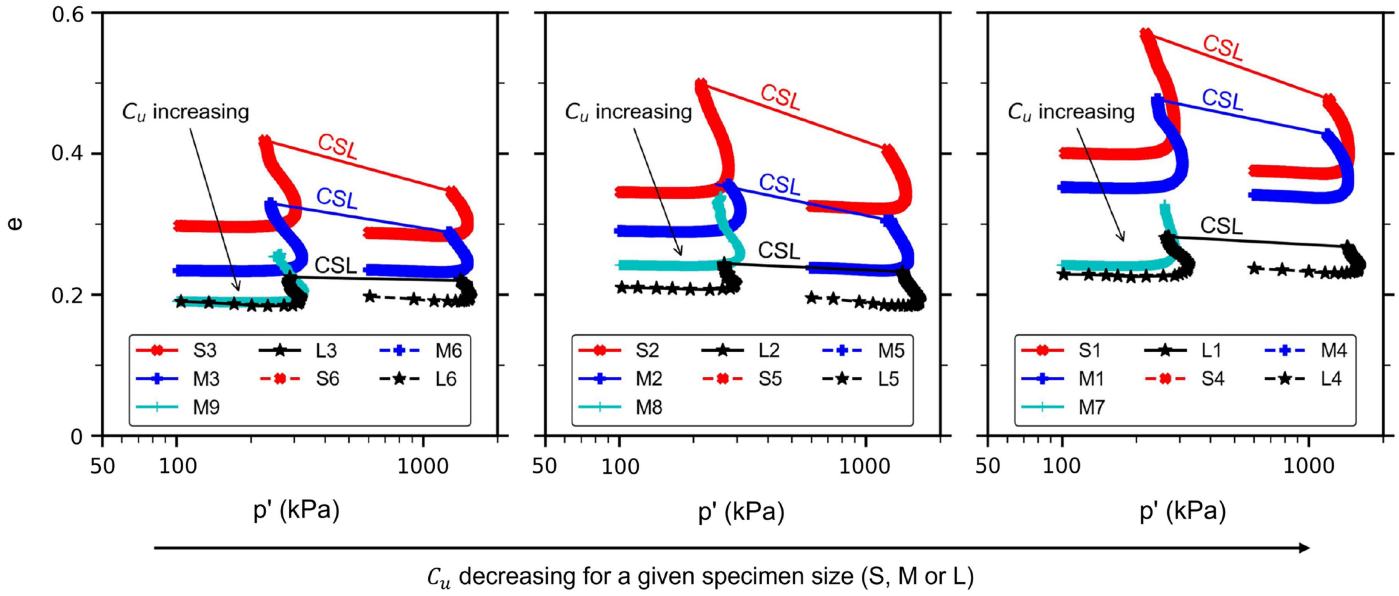

Fig. 18. Dilatancy paths in $e - p'$ space and estimated CSL for all the tests.

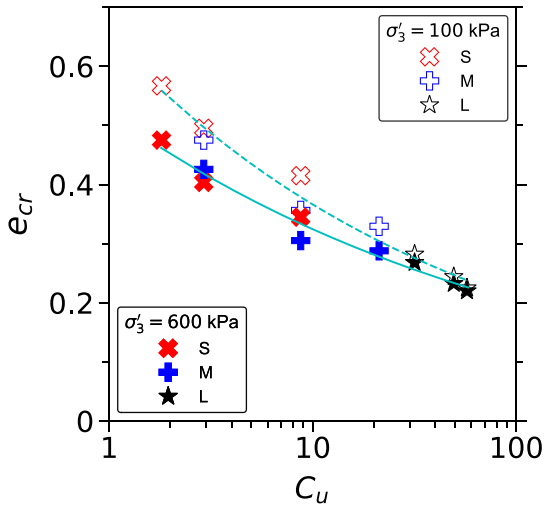

Fig. 19. Estimated critical state void ratio e_{cr} versus C_u for all the tests on scalped specimens (dashed and solid lines for power fitting of tests at $\sigma'_3 = 100$ and 600 kPa, respectively).

using scalping grading and truncation techniques, with C_u spanning between 1.8 and 57.3 across 10 distinct particle size distributions. The testing program involved three devices with distinct diameters: S specimens of $D = 100$ mm, M specimens of $D = 150$ mm, and L specimens with $D = 800$ mm. The results were evaluated in terms of dilatancy, strain modulus, peak shear strength, and critical states. The following conclusions can be drawn from the test results:

- Scaling a coarse material results in a more uniformly graded smaller specimen, which affects its volumetric dilatancy. Due to grading effects, dense small-scale specimens at equivalent relative densities exhibit higher dilatancy and critical state void ratio than the original coarse soil.
- While volumetric dilatancy increases in small-scale specimens, their peak strength decreases 3° to 4° compared to the coarser material. Therefore, using small specimens represents a slightly conservative approach in terms of strength. However, this trend could be reversed if the amount of particle crushing becomes significant, due to size effects on particle fragmentation resistance.
- Under substantial maximum grain size reductions—using grain size scaling factors up to 25 and a reduction in C_u by approximately 30 times—the scattering around the secant modulus E_{50} showed about 15% to 30% variation at low confining stress (100 kPa) and remained practically unchanged at higher stress levels (600 kPa).

Building on previous studies by several researchers, including the authors, the results presented in this paper offer insights that support the following recommendations for practitioners:

- Since scaling granular soils inherently alters grading, it is advisable to characterize specimens at different scales under equivalent relative density conditions. However, this approach is often challenged by the presence of oversized particles and the current lack of standardized procedures for determining the maximum and minimum densities of coarse-grained or oversized materials. Thus, extrapolation of results may be unavoidable in practical applications.
- Particle shape can significantly influence the results of small-scale tests on granular soils. Therefore, it is important to measure grain shapes across all grain sizes involved and compare them with the original coarse soil being scaled. If the finer grains are more angular than the coarse fraction, the resulting small-scale specimens may exhibit greater volumetric dilatancy and higher shear strength due to increased particle interlocking, leading to optimistic material parameters for the original coarse material. In contrast, an inverse correlation between size and grain angularity can result in conservative mechanical characterizations.
- If the primary objective of an experimental program is to characterize the prepeak behavior of dense coarse soils, the results of this study suggest that the scalping method can provide reasonable approximations within the examined grading ranges. Material testing at different scales is strongly recommended; however, the expected variations in secant stiffness and peak strength across specimen scales are relatively small and can be typically accounted for by standard safety factors.

- If postpeak behavior is the focus, the influence of grading on dilatancy becomes a critical consideration during constitutive model calibration using data from small-scale specimens, since often dilatancy serves as a key criterion that significantly impacts the conclusions drawn from numerical modeling. To avoid overestimation or underestimation of limit states, it is essential to incorporate a realistic particle size distribution whenever feasible. Also, the enhanced dilatancy observed in small-scale dense specimens implies that critical state behavior may not be achieved within the strain limits of conventional triaxial testing. In such cases, testing specimens in a loose state is advisable, as it may help mitigate this effect. Moreover, if particle shape remains essentially unchanged in the small-scale specimens, extensive empirical evidence suggests that the critical friction angle is relatively insensitive to grading. Therefore, loose small-scale specimens may provide a reliable basis for assessing shear strength at large strains.
- Although particle crushing was not significant in this study, caution is advised under high-stress conditions, particularly for blasted and crushed rockfill, which are more prone to crushing than alluvial gravels. When the applied stress approaches the characteristic crushing strength of the grains, particle breakage can become significant, affecting both compressibility and peak strength. As with any brittle solid, the probability of encountering internal flaws that initiate breakage of a grain increases with its size. Consequently, finer particles are inherently stronger, and small-scale specimens tend to experience less grain crushing. Thus, scaling may lead to higher peak strength compared to the original coarser material, potentially yielding optimistic mechanical parameters for design.

Many uncertainties remain regarding the effects of small-scale testing. Future research directions include studying size effects on granular materials with nonnegligible fine fractions (<80 μm), incorporating loose conditions, analyzing different stress paths, and investigating materials that are highly sensitive to particle crushing. More extensive investigations are also required to assess the different percentages of replaced coarse fraction in the truncation technique, in order to establish a threshold value that allows reliable comparison with the scalping grading method. Finally, although rare and expensive, large-scale testing will still provide valuable information that will contribute to a better understanding of coarse soils.

Data Availability Statement

Data from all tests presented in this work are available in the following repository: https://zenodo.org/records/16699865.

Acknowledgments

This research work was possible thanks to the financial support of the Mitacs Globalink scholarship (Ref. FR118496), the Institute of Soil Mechanics and Rock Mechanics (IBF) at Karlsruhe Institute of Technology, the Natural Sciences and Engineering Research Council of Canada (NSERC) (Ref. RGPIN-2019-06118), the Fonds de recherche du Québec—Nature et technologies (FRQNT) through the 'Programme de recherche en partenariat sur le développement durable du secteur minier-II' (Ref. 2020-MN-281267), and the industrial partners of the Research Institute on Mines and the Environment (RIME) (irme.ca/en). Gilbert Girumugisha would also like to acknowledge Pia Gölz, Nebil Demiral and Henning Borowski for the technical support. In addition, the use of parts of the datasets and the investigated soil was allowed by Gruner AG, Basel.

Author Contributions

Gilbert Girumugisha: Conceptualization; Data curation; Formal analysis; Investigation; Methodology; Resources; Validation; Visualization; Writing – original draft. Carlos Ovalle: Conceptualization; Formal analysis; Funding acquisition; Investigation; Methodology; Project administration; Resources; Supervision; Validation; Writing – original draft; Writing – review and editing. Holger Reith: Conceptualization; Data curation; Formal analysis; Investigation; Methodology. Hans Henning Stutz: Conceptualization; Formal analysis; Investigation; Methodology; Project administration; Resources; Supervision; Validation; Writing – review and editing.

References

Ahmed, S. S., A. Martinez, and J. T. DeJong. 2023. "Effect of gradation on the strength and stress-dilation behavior of coarse-grained soils in drained and undrained triaxial compression." *J. Geotech. Geoenviron. Eng.* 149 (5): 04023019. https://doi.org/10.1061/JGGEFK.GTENG-10972.

Al-Hussaini, M. M. 1970. *The influence of end restraint and method of consolidation on the drained triaxial compressive strength of crushed napa basalt*. Vicksburg, MS: US Army Engineer Waterways Experiment Station.

Al-Hussaini, M. M. 1983. "Effect of particle size and strain conditions on the strength of crushed basalt." *Can. Geotech. J.* 20 (4): 706–717. https://doi.org/10.1139/t83-077.

Amirpour Harehdasht, S., M. Karray, M. N. Hussien, and M. Chekired. 2017. "Influence of particle size and gradation on the stress-dilatancy behavior of granular materials during drained triaxial compression." *Int. J. Geomech.* 17 (9): 04017077. https://doi.org/10.1061/(ASCE)GM.1943-5622.0000951.

ASTM. 2017. *Standard practice for classification of soils for engineering purposes (unified soil classification system)*. ASTM D2487. West Conshohocken, PA: ASTM.

Barton, N., and B. Kjærnsli. 1981. "Shear strength of rockfill." *J. Geotech. Eng. Div.* 107 (7): 873–891. https://doi.org/10.1061/AJGEB6.0001167.

Biarez, J., and P.-Y. Hicher. 1994. *Elementary mechanics of soil behaviour: Saturated remoulded soils*. Rotterdam, Netherlands: A.A. Balkema.

Biarez, J., and P.-Y. Hicher. 1997. "Influence de la granulométrie et de son évolution par ruptures de grains sur le comportement mécanique de matériaux granulaires." *Revue française de génie civil* 1 (4): 607–631. https://doi.org/10.1080/12795119.1997.9692147.

Bolton, M. D. 1986. "The strength and dilatancy of sands." *Géotechnique* 36 (1): 65–78. https://doi.org/10.1680/geot.1986.36.1.65.

Brauns, J., and K. Kast. 2007. "Dynamic compaction of rockfill samples." In *Proc., 10th Int. Conf. on Soil Mechanics and Foundation Engineering*, edited by H. I. Ling, L. Callisto, D. Leshchinsky, and J. Koseki, 669–671. Rotterdam, Netherlands: A. A. Balkema.

Brauns, J., and H. Reith. 2000. "Testing the stress-strain properties and the shear strength of rockfill material." *Int. J. Hydropower Dams* 7 (1): 62–63.

Cantor, D., E. Azema, F. Radjai, and P. Sornay. 2018. "Rheology and structure of polydisperse three-dimensional packings of spheres." *Phys. Rev. E* 98 (5): 052910. https://doi.org/10.1103/PhysRevE.98.052910.

Cantor, D., and C. Ovalle. 2025. "Sample size effects on the critical state shear strength of granular materials with varied gradation and the role of column- like local structures." *Géotechnique* 75 (1): 29–40. https://doi.org/10.1680/jgeot.23.00032.

Carrasco, S., D. Cantor, C. Ovalle, and F. Dubois. 2025. "Particle shape distribution effects on the critical strength of granular materials." *Comput. Geotech.* 177 (Jan): 106896. https://doi.org/10.1016/j.compgeo.2024.106896.

Carrasco, S., D. Cantor, C. Ovalle, and P. Quiroz. 2023. "Shear strength of angular granular materials with size and shape polydispersity." *Open Geomech.* 4 (Sep): 1–4. https://doi.org/10.5802/ogeo.15.

Daouadji, A., P.-Y. Hicher, and A. Rahma. 2001. "An elastoplastic model for granular materials taking into account grain breakage." *Eur. J. Mech. A. Solids* 20 (1): 113–137. https://doi.org/10.1016/S0997-7538(00)01130-X.

Deiminiat, A., L. Li, and F. Zeng. 2022. "Experimental study on the minimum required specimen width to maximum particle size ratio in direct shear tests." *CivilEng* 3 (1): 66–84. https://doi.org/10.3390/civileng3010005.

Deng, Y., Y. Yilmaz, A. Gokce, and C. S. Chang. 2021. "Influence of particle size on the drained shear behavior of a dense fluvial sand." *Acta Geotech.* 16 (7): 2071–2088. https://doi.org/10.1007/s11440-021-01143-7.

DIN (Deutsches Institut für Normung). 2022. *Baugrund, Untersuchung von Bodenproben-Bestimmung der Dichte nicht bindiger Boden bei lockerster und dichtester Lagerung. Standard test method for minimum and maximum densities*. [In German.] DIN 18126. Berlin: Deutsches Institut für Normung, Beuth Verlag GmbH.

Girumugisha, G., C. Ovalle, and S. Ouellet. 2024. "Grading scalping and sample size effects on critical shear strength of mine waste rock through laboratory and in-situ testing." *Int. J. Rock Mech. Min. Sci.* 183 (Nov): 105915. https://doi.org/10.1016/j.ijrmms.2024.105915.

Hao, S., and T. Pabst. 2023. "Mechanical characterization of coarse-grained waste rocks using large-scale triaxial tests and neuroevolution of augmenting topologies." *J. Geotech. Geoenviron. Eng.* 149 (6): 04023039. https://doi.org/10.1061/JGGEFK.GTENG-10721.

Hardin, B. 1985. "Crushing of soil particles." *J. Geotech. Eng.* 111 (10): 1177–1192. https://doi.org/10.1061/(ASCE)0733-9410(1985)111:10(1177).

Hassan, N. A., N. S. Nguyen, D. Marot, and F. Bendahmane. 2022. "Consequences of scalping and scalping/replacement procedures on strength properties of coarse-grained gap-graded soils." *Can. Geotech. J.* 59 (10): 1819–1832. https://doi.org/10.1139/cgj-2021-0504.

Hettler, A., and I. Vardoulakis. 1984. "Behaviour of dry sand tested in a large triaxial apparatus." *Géotechnique* 34 (2): 183–197. https://doi.org/10.1680/geot.1984.34.2.183.

Hu, W., C. Dano, P.-Y. Hicher, J.-Y. Le Touzo, F. Derkx, and E. Merliot. 2011. "Effect of sample size on the behavior of granular materials." *Geotech. Test. J.* 34 (3): 186–197. https://doi.org/10.1520/GTJ103095.

Kikumoto, M., D. M. Wood, and A. Russell. 2010. "Particle crushing and deformation behaviour." *Soils Found.* 50 (4): 547–563. https://doi.org/10.3208/sandf.50.547.

Leussink, H. 1960. Vol. 1 of *Bau eines grossen dreiaxialen shergerätes zur untersuchung grobkörniger erdstoffe (Design of a large triaxial shear apparatus for investigating coarse grained soils)*. Karlsruhe, Germany: Soil Mechanics Institute of the Karlsruhe Technical Univ. Germany.

Li, G., C. Ovalle, C. Dano, and P.-Y. Hicher. 2013. "Influence of grain size distribution on critical state of granular materials." In *Constitutive modeling of geomaterials*, edited by Q. Yang, J.-M. Zhang, H. Zheng, and Y. Yao, 207–210. Berlin: Springer.

Linero, S., E. Azema, N. Estrada, S. Fityus, J. Simmons, and A. Lizcano. 2019. "Impact of grading on steady-state strength." *Géotech. Lett.* 9 (4): 328–333. https://doi.org/10.1680/jgele.18.00216.

Linero, S., L. Bradfield, S. G. Fityus, J. V. Simmons, and A. Lizcano. 2020. "Design of a 720-mm square direct shear box and investigation of the impact of boundary conditions on large-scale measured strength." *Geotech. Test. J.* 43 (6): 1463–1480. https://doi.org/10.1520/GTJ20190344.

Linero, S., S. Fityus, J. Simmons, A. Lizcano, and J. Cassidy. 2017. "Trends in the evolution of particle morphology with size in colluvial deposits overlying channel iron deposits." *EPJ Web Conf.* 140 (Jun): 14005. https://doi.org/10.1051/epjconf/201714014005.

Linero, S., C. Palma, and R. Apablaza. 2007. "Geotechnical characterisation of waste material in very high dumps with large scale triaxial testing." In *Proc., 2007 Int. Symp. on Rock Slope Stability in Open Pit Mining and Civil Engineering*, edited by Y. Potvin, 59–75. Perth, WA, Australia: Australian Centre for Geomechanics. https://doi.org/10.36487/ACG_repo/708_2.

Liu, J., D. Zou, X. Kong, and H. Liu. 2016. "Stress-dilatancy of zipingpu gravel in triaxial compression tests." *Sci. China Technol. Sci.* 59 (2): 214–224. https://doi.org/10.1007/s11431-015-5919-8.

Lowe, J. 1964. "Shear strength of coarse embankment dam materials." In Vol. 3 of *Proc., 8th Int. Congress on Large Dams*, 745–761. Paris: International Commission on Large Dams.

Marachi, N. D., C. K. Chan, and H. B. Seed. 1972. "Evaluation of properties of rockfill materials." *J. Soil Mech. Found. Div.* 98 (1): 95–114. https://doi.org/10.1061/JSFEAQ.0001735.

Marsal, R. J. 1967. "Large scale testing of rockfill materials." *J. Soil Mech. Found. Div.* 93 (2): 27–43. https://doi.org/10.1061/JSFEAQ.0000958.

Matsuoka, H., S. Liu, D. Sun, and U. Nishikata. 2001. "Development of a new in-situ direct shear test." *Geotech. Test. J.* 24 (1): 92–102. https://doi.org/10.1520/GTJ11285J.

Muir Wood, D., and K. Maeda. 2008. "Changing grading of soil: Effect on critical states." *Acta Geotech.* 3 (1): 3–14. https://doi.org/10.1007/s11440-007-0041-0.

Ning, F., J. Liu, D. Zou, X. Kong, and G. Cui. 2024. "Super-large-scale triaxial tests to study the effects of particle size on the monotonic stress–strain response of rockfill materials." *Acta Geotech.* 20 (4): 1847–1858. https://doi.org/10.1007/s11440-024-02471-0.

Osses, R., J. Pineda, C. Ovalle, S. Linero, and E. Sáez. 2024. "Scale and suction effects on compressibility and time-dependent deformation of mine waste rock material." *Eng. Geol.* 340 (Oct): 107668. https://doi.org/10.1016/j.enggeo.2024.107668.

Ovalle, C., and C. Dano. 2020. "Effects of particle size–strength and size–shape correlations on parallel grading scaling." *Géotech. Lett.* 10 (2): 191–197. https://doi.org/10.1680/jgele.19.00095.

Ovalle, C., E. Frossard, C. Dano, W. Hu, S. Maiolino, and P.-Y. Hicher. 2014. "The effect of size on the strength of coarse rock aggregates and large rockfill samples through experimental data." *Acta Mech.* 225 (8): 2199–2216. https://doi.org/10.1007/s00707-014-1127-z.

Ovalle, C., and P.-Y. Hicher. 2020. "Modeling the effect of wetting on the mechanical behavior of crushable granular materials." *Geosci. Front.* 11 (2): 487–494. https://doi.org/10.1016/j.gsf.2019.06.009.

Ovalle, C., S. Linero, C. Dano, E. Bard, P.-Y. Hicher, and R. Osses. 2020. "Data compilation from large drained compression triaxial tests on coarse crushable rockfill materials." *J. Geotech. Geoenviron. Eng.* 146 (9): 06020013. https://doi.org/10.1061/(ASCE)GT.1943-5606.0002314.

Polanía, O., M. Cabrera, M. Renouf, E. Azéma, and N. Estrada. 2023. "Grain size distribution does not affect the residual shear strength of granular materials: An experimental proof." *Phys. Rev. E* 107 (5): L052901. https://doi.org/10.1103/PhysRevE.107.L052901.

Quiroz-Rojo, P., D. Cantor, M. Renouf, C. Ovalle, and E. Azéma. 2024. "Rev assessment of granular materials with varied grading based on macro- and micro-mechanical statistical data." *Acta Geotech.* 20 (Apr): 1585–1598. https://doi.org/10.1007/s11440-024-02498-3.

Schanz, T., and P. A. Vermeer. 1996. "Angles of friction and dilatancy of sand." *Géotechnique* 46 (1): 145–151. https://doi.org/10.1680/geot.1996.46.1.145.

Schanz, T., and P. A. Vermeer. 1998. "On the stiffness of sands." In *Pre-failure deformation behaviour of geomaterials*, 383–387. London: Thomas Telford.

Strahler, A., A. W. Stuedlein, and P. W. Arduino. 2016. "Stress-strain response and dilatancy of sandy gravel in triaxial compression and plane strain." *J. Geotech. Geoenviron. Eng.* 142 (4): 04015098. https://doi.org/10.1061/(ASCE)GT.1943-5606.0001435.

Varadarajan, A., K. G. Sharma, K. Venkatachalam, and A. K. Gupta. 2003. "Testing and modeling two rockfill materials." *J. Geotech. Geoenviron. Eng.* 129 (3): 206–218. https://doi.org/10.1061/(ASCE)1090-0241(2003)129:3(206).

Verdugo, R., and K., de la Hoz. 2007. "Strength and stiffness of coarse granular soils." In *Soil stress-strain behavior: Measurement, modeling and analysis*, edited by H. I. Ling, L. Callisto, D. Leshchinsky, and J. Koseki, 243–252. Dordrecht, Netherlands: Springer Netherlands.

Wang, X., B. Xu, X. Meng, and Q. Fan. 2022. "Experimental study on the dilatancy characteristics and equation of saturated sand–gravel composites during the whole shearing process." *Int. J. Geomech.* 22 (3): 04021310. https://doi.org/10.1061/(ASCE)GM.1943-5622.0002306.

Xiao, Y., H. Liu, Y. Chen, and J. Jiang. 2014. "Strength and deformation of rockfill material based on large-scale triaxial compression tests. I: Influences of density and pressure." *J. Geotech. Geoenviron. Eng.* 140 (12): 04014070. https://doi.org/10.1061/(ASCE)GT.1943-5606.0001176.

Xiao, Y., H. Liu, W. Zhang, H. Liu, F. Yin, and Y. Wang. 2016. "Testing and modeling of rockfill materials: A review." *J. Rock Mech. Geotech. Eng.* 8 (3): 415–422. https://doi.org/10.1016/j.jrmge.2015.09.009.

Xiao, Y., C. Wang, H. Wu, and C. S. Desai. 2021. "New simple breakage index for crushable granular soils." *Int. J. Geomech.* 21 (8): 04021136. https://doi.org/10.1061/(ASCE)GM.1943-5622.0002091.

Yan, W. M., and J. Dong. 2011. "Effect of particle grading on the response of an idealized granular assemblage." *Int. J. Geomech.* 11 (4): 276–285. https://doi.org/10.1061/(ASCE)GM.1943-5622.0000085.

Yang, J., and X. D. Luo. 2018. "The critical state friction angle of granular materials: Does it depend on grading?" *Acta Geotech.* 13 (3): 535–547. https://doi.org/10.1007/s11440-017-0581-x.

Zeller, J., and R. Wullimann. 1957. "The shear strength of the shell materials for the Go-schenenalp Dam, Switzerland." In Vol. 2 of *Proc., 4th Int. Conf. on Soil Mechanics and Foundation Engineering*, 399–415. London: International Society of Soil Mechanics and Foundation Engineering.

Zhang, T., Y. Wang, C. Zhang, and S. Wang. 2024. "DEM investigation of particle gradation effect on the stress-dilatancy behavior of granular soil." *Adv. Powder Technol.* 35 (11): 104692. https://doi.org/10.1016/j.apt.2024.104692.

Zheng, J., and R. D. Hryciw. 2015. "Traditional soil particle sphericity, roundness and surface roughness by computational geometry." *Géotechnique* 65 (6): 494–506. https://doi.org/10.1680/geot.14.P.192.